Hindawi Publishing Corporation
EURASIP Journal on Image and Video Processing
Volume 2009, Article ID 217016, 13 pages
doi:10.1155/2009/217016

Research Article

A New Technique for the Digitization and Restoration of Deteriorated Photographic Negatives

George V. Landon,[1] Duncan Clarke,[2] and W. Brent Seales[3]

[1] *Department of Computer Science, Eastern Kentucky University, Richmond, KY 40475, USA*
[2] *Fremont Associates, LLC, Camden, SC 29020-4316, USA*
[3] *Center for Visualization and Virtual Environments, Computer Science Department, University of Kentucky, Lexington, KY 40506-0495, USA*

Correspondence should be addressed to George V. Landon, george.landon@eku.edu

Received 17 February 2009; Revised 12 June 2009; Accepted 31 August 2009

Recommended by Nikos Nikolaidis

This work describes the development and analysis of a new image-based photonegative restoration system. Deteriorated acetate-based safety negatives are complex objects due to the separation and channeling of their multiple layers that has often occurred over 70 years time. Using single-scatter diffuse transmission model, the intrinsic intensity information and shape distortion of film can be modeled. A combination of structured-light and high-dynamic range imaging is used to acquire the data which allows for automatic photometric and geometric correction of the negatives. This is done with a simple-to-deploy and cost-effective camera and LCD system that are already available to most libraries and museums. An initial analysis is provided to show the accuracy of this method and promising results of restoration of actual negatives from a special archive collection are then produced.

1. Introduction

Much of the current research in the area of document imaging has focused in document acquisition and restoration and, in particular, digitizing bound books or manuscript pages. Acquisition and restoration of general document types has been given focus by many groups who have made a great deal of progress in creating fast and accurate digitization systems. Currently, restoration of standard documents typically consists of correcting geometric and photometric distortions. Some works have focused mainly on geometric correction of distorted documents [1, 2]. Other projects have focused more on photometric correction of documents [3, 4], while others have relied on assumed document shapes to provide photometric and geometric corrections for objects such as bound books [5] and folded documents [6]. Research has also been performed to scan documents that are not typically visible with normal imaging devices [7]. However, deteriorated photographic negatives have typically been overlooked. Digitally preserving and restoring these deteriorating negatives is an urgent challenge that requires an easily-accessible solution since many of them are suffering devastating forms of deterioration [8].

A significant contribution of work has focused on the restoration of deteriorated photographs. Digital Inpainting [9] provides an efficient procedure for restoring areas of loss in digital images. Inpainting has been improved in many ways since [10–12], however, these procedures assume total loss of data in areas requiring restoration. Content-based representation was used to assist in automatic and semiautomatic restorations [13]. Reflective light imaging has also been used to detect blotches that have not fully destroyed the underlying content [14]. Once detected, the content is extracted from the blotches to remove the deterioration. In a slightly different direction, a technique was developed to remove reflections from within the photographic content itself [15]. For an overview of photograph restoration techniques, the reader may refer to [16]. In more recent work, a flatbed scanner was utilized to detect surface variations in a photograph caused by folding [17]. While the reconstruction technique works well for detecting anomalies, the restoration uses inpainting techniques that are not suitable for large areas

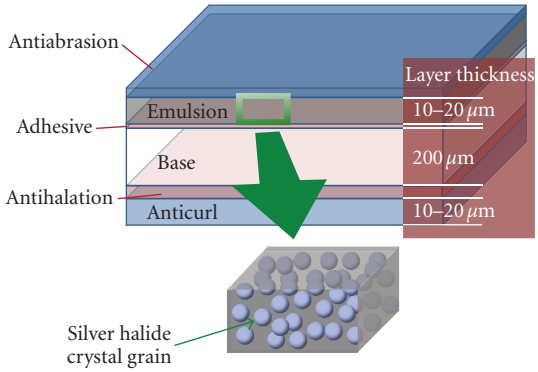

Figure 1: The physical composition of film.

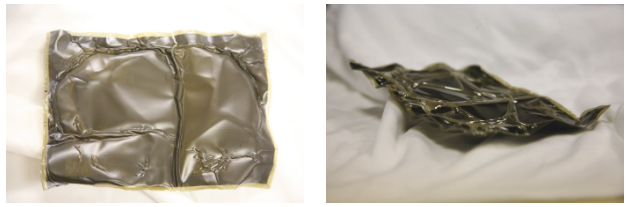

(a) The emulsion side of a deteriorated negative

(b) The acetate side of the same negative

Figure 2: Example of a severely damaged negative.

of deterioration. Moreover, most of these methods generally focus on a scanned image of a photograph and usually only handle standard photographic prints. One project that does work directly with glass plate negatives [18] uses rigid transformations to assemble broken photographs.

While these works have provided a great deal of progress toward acquiring many types of documents, they do not provide a way to capture documents with nonlinear transparent properties. However, there has been work to acquire shape and optical properties of general transparent objects. One technique makes assumptions about the object shape to reconstruct the surface [19]. In contrast, another method, using scatter tracing [20], acquires the outermost surface of complex transparent objects using assumptions about the object composition. More recently, heat was used as a structured-light illuminant to accurately scan complex objects [21]; however, this type of technique is unsuitable for delicate pieces under conservation. For some applications, recording only the light transport of a scene is required. Specifically, environment matting [22, 23] uses a novel method for capturing the light transport through a scene. The work presented here extends initial attempts at negative scanning developed by the authors [24]. However, to the authors' knowledge, no other work has been directly performed on the damaged acetate negatives.

2. Damage and Restoration

The basic composition of film is shown in Figure 1. The two most important components to be considered in the research presented here are the emulsion layer and base layer. The emulsion layer contains the photographic content of the film, while the base layer provides support and rigidity to the film. Therefore, the base layer itself contains no relevant information but only provides the physical stability necessary to keep the emulsion structurally sound.

The damage to film collections is widespread and increasing [8]. It was once thought that the deterioration of various laminate layers of photographic negatives, which would make the negative unprintable, was isolated to a very narrow set dating from the late 1940s to early 1950s. It has since been discovered, however, that the number of degraded negatives is much higher and covers a broader period of time, from 1925 to as late as 1955. This period of 30 years encompasses vast and diverse collections of "safety" negatives. These negatives were produced from new materials in order to move away from the flammability of cellulose nitrate, which was used for still photography until the early 1920s and in the motion picture industry well into the 1950s. The safety film that emerged was varied in its composition but largely based on cellulose diacetate. This new material lessened the risk of flammability but was not an ideal film base because of its tendency, even under proper conservation, to absorb moisture and cause dimensional distortion, as shown in Figure 2. Eventually new polyester-based material was developed in the 1950s to solve the dimensional instability problem. However, the diacetate period produced millions of negatives that are now at risk.

The worldwide response by conservators to the risk of damage to collections is not handled uniformly. In the best case, institutions have recognized deterioration and have taken steps to store collections in a controlled environment to minimize the progressive damage, but the chemical deterioration of the acetate base can only be slowed, not stopped. The size and importance of the affected photographic collections cannot be overstated, with many individual collections containing over 100 000 negatives. The reality of budgeting, space constraints, and personnel limitations has led to a situation where damage is continuing and has placed many important items at risk. This has created an urgent need for a technique that can capture the information in each of the negatives of a large collection before the damage causes a complete and irretrievable loss of information.

2.1. Restoration Approaches. The primary approach to slowing the deterioration of photographic negatives is correct conservation. For many collections, it is simply too late and the damage has already been done. At the present, the only known solution to repair a deteriorating negative is to strip the emulsion layer from the degraded film base and either reattach or duplicate it onto another sheet of film [8]. This is an irreversible physical process that is labor intensive and expensive. However, it does solve the problem because the flattened emulsion layer, which contains the photographic information, becomes distortion free with a destructive physical separation of the layers [25].

The print (or digitization, which is the creation of a digital image of the emulsion) from a damaged negative is distorted in two primary ways. First, the damaged acetate becomes opaque where it has separated from the emulsion. This introduces attenuation when light passes through the material. We term this distortion of intensities a *photometric* distortion. Second, the dimensional instability causes the negative to become nonplanar. Since it cannot lay flat its content is distorted when light is projected through it onto another surface. This is a *geometric* distortion which could be removed if the negatives were somehow made to lay flat.

2.2. Digital Restoration. In contrast to physical restoration, we present a tool for the *digital* restoration of photographic negatives. While physical restoration is always an option, there are three key benefits to a noninvasive, purely digital approach. First, the digital approach creates a digitized model, which is often the desired goal even when the negative is not yet damaged. The digital model stores information content without being subject to further damage. Second, in contrast to physical restoration, the digital process leaves the original negative in its current state, meaning that conservation can continue and no changes are made that are irreversible. If the results from a digital approach are not acceptable, the more challenging and expensive physical approach can still be applied. Third, the approach can be automated, opening the possibility of streamlined workflow to capture large collections in their entirety. It is extremely costly and time-intensive to physically restore a large collection in its entirety.

The two primary effects resulting from the physical damage of the photographic negative must be overcome in order to engineer a process that can restore an image of the emulsion layer without the need to physically separate and reseat the emulsion layer. We can model these effects individually and we describe the essential points in the following sections.

2.2.1. Photometric. The photographic information is found in the emulsion layer of the negative. As light passes through this layer, areas with higher silver halide density absorb more light. Variations across the layer encode the information that makes up the "picture." We designate this information as "photometric" in the sense that the intensity variations along the emulsion layer are the crucial photometric property to be captured. Any damage to this layer or to anything that might block the ability to correctly record these intensity variations will cause a photometric distortion. In the case of damaged acetate, the light is not transmitted at a constant intensity across the emulsion because the separated acetate attenuates the light that would otherwise pass through that portion of the emulsion. The result is an artifact or a photometric distortion of the emulsion information.

2.2.2. Geometric. The correct, original shape of the emulsion layer is a plane. Damaged negatives are no longer planar, which creates a geometric distortion when the negative is printed using a standard light table. These distortions are directly related to the nonplanar shape of the negative and are largely independent of the content of the emulsion. In other words, a negative that is non-planar but without reduced transmission will create a print that is photometrically correct but has content that shows non-linear distortions.

It is important that the photometric and geometric distortions can be treated separately, leading to a complete solution framework for digital restoration.

3. Image-Based Modeling of the Negative Restoration

For some document types, full three-dimensional reconstruction is either unnecessary or impractical when attempting digitization and restoration. Many historical documents contain wrinkles, creases, and other high-frequency features either beyond the accuracy of many 3D scanners or requiring time intensive acquisition procedures. In these cases, a more appropriate approach is to work in a pixel-by-pixel image-based acquisition and restoration methodology. This work develops that methodology by assembling a cost-effective scanning system comprised of a laptop to emulate a *smart* light-table and a camera to observe illumination changes in the scene.

The area of material model formulation, using image-based methods, and rendering has been a widely researched area in computer graphics. Wang et al. [26] produced a real-time renderer of plant leaves that included global illumination effects. This work is of particular interest due to the application of an image-based acquisition technique to reconstruct the transmissiveness and reflectivity of the leaves. Devices have been built to acquire the material properties of various types of documents and other materials. Gardner et al. [27] introduce a linear light source gantry that obtains a Bidirectional Reflectance Distribution Function (BRDF) of an object while providing depth and opacity estimates. Also, Mudge et al. [28] use a *light dome* to obtain reflectance properties of various materials. These works, and many others, show the possibilities of photorealistic rendering of acquired objects. However, the purpose of our proposed work is not to realistically render a material but to restore a negative to its original form by estimating the material changes caused by deterioration.

The technique presented here exploits the transmissiveness of negatives to obtain a model of the document that allows complete reconstruction of the intrinsic color, content, and distorted shape. Also, to reduce the burden of the system operator, there is minimal calibration required before scanning can begin unlike many other document digitization systems mentioned in Section 1.

The transmissive document scanner is designed to accurately digitize and even restore content that is marred by damage and age. The photometrically corrected content is extracted directly during the scanning process while working in a completely image-based realm. Moreover, the obtained shape information can be used to restore the shape of a geometrically warped surface with restoration

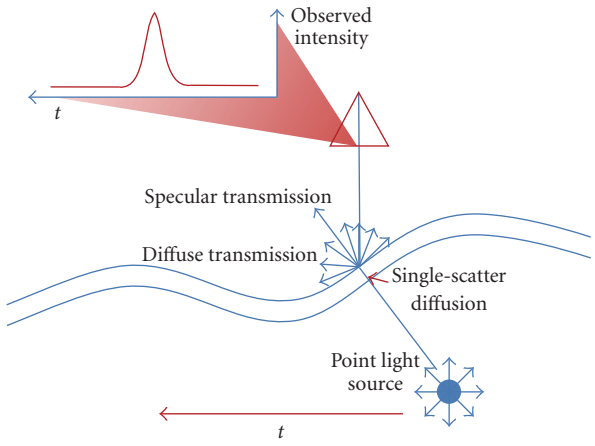

Figure 3: Diffuse single-scatter transmission of a back-lit light source.

procedures described in Section 4.3.2. Consequently, image-based techniques provide a direct way to generate restored images without requiring metric reconstructions that add to overall system complexity.

3.1. Physical Model. The solution presented here works on the premise that the composition of most document substrates is composed of numerous nonuniformly aligned homogeneous elements. Consequently, the typical composition of document substrates follows a highly isotropic scattering of transmitted light. The silver halide grains of the emulsion layer in a photonegative, by design, create a diffuse transmission of light.

The scanning method presented here will focus on diffuse transmission. For a single-layer document, the diffuse transmission of light can be approximated as a single-scatter diffusion. Chandresakar [29] provides an approximation of the single-scattering that occurs in diffuse transmission as

$$L_t = L_i e^{-\tau/\cos\theta_t} + \frac{1}{4\pi}\phi_0 L_i \frac{\cos\theta_i}{\cos\theta_t + \cos\theta_i}\left(e^{-\tau/\cos\theta_t} - e^{-\tau/\cos\theta_i}\right), \tag{1}$$

where θ_i is the angle between the surface normal and incident light, θ_t is the angle between outgoing light and the surface normal, ϕ_0 is the phase function, L_i is the incident light intensity, and τ is the material thickness.

The single-scatter transmission has been well studied in the area of computer graphics. Frisvad et al. [30] use Chandrasekhar's work to create an efficient rendering system for thin semitransparent objects. Moreover, the area of plant/leaf rendering has been thoroughly studied [26, 31, 32] with respect to single-scatter transmission. In a more recent work, Gu et al. [33] model and render a thin layer of distortions caused by dirt on a surface using fully acquired BRDF and Bidirectional Transmission Distribution Function (BTDF) functions.

Figure 3 shows a particular case where a light source is translated approximately parallel to semiplanar object. For a single-pixel observation, as the light translates, the intensity follows a cosine-like response where the light is incident at an angle parallel to the surface normal. The incoming illumination angle can be calculated as $\cos\theta_i = \omega_i \cdot n$ where ω_i is the incident light direction and n is the outward surface normal. Moreover, in the case of diffuse transmission, an assumption can be made that the greatest transmitted intensity will occur when $\omega_i \simeq n$. Therefore, for the purpose of this work, $\cos\theta_i$ will be approximated as 1.

For diffuse materials, it is safe to model the material as a translucent material with a highly diffuse transmission of light. Therefore, the phase function can be modeled with isotropic scattering; thus ϕ_0 becomes a constant 1. The direct transmission can be safely ignored for highly diffuse materials, and so single-scattering becomes the only factor in light transmission through the material. Considering these assumptions, 1 can be approximated as

$$L_t = \frac{1}{4\pi} L_i \frac{1}{\cos\theta_t + 1}\left(e^{-\tau/\cos\theta_t} - e^{-\tau}\right), \tag{2}$$

where $\cos\theta_t$ is the only varying quantity across the surface while τ and L_i remain constant.

The intensity increase generated when the incident light angle, ω_i, becomes parallel with the surface normal n will be used to estimate the shape of the document surface. However, for documents that are mostly specular transmissive, directly transmit light, surface normal no longer plays a large role in the intensity of transmitted light. Therefore, the following scanning process only works well for documents that exhibit diffuse transmission.

This diffuse transmission can be modeled with the BTDF:

$$f_t(\omega_i, \omega_t) = \frac{L_t(\omega_t)}{L_i(\omega_i)\cos\theta_i d\omega_i}, \tag{3}$$

where ω_i is the incident light direction, ω_t is the transmitted light direction, $L_i(\omega_i)$ is the quantity of light arrive from ω_i, $L_t(\omega_t)$ is the quantity of light transmitted along ω_t, and $d\omega_i$ is the differential solid angle. When two BTDFs are estimated and at least one property remains constant between them, a direct comparison can then be made between two distinct scenes. In this case, the incident light maintains constant flux since the sweeping illuminant repeats with the same properties in both scenes:

$$\frac{L_t(\omega_t)}{f_t(\omega_i, \omega_t)\cos\theta_i d\omega_i} = \frac{L_t'(\omega_t)}{f_t'(\omega_i', \omega_t)\cos\theta_i' d\omega_i'}. \tag{4}$$

Therefore, we now have two disparate cases that are modeled by the BTDF for each small region imaged by a camera pixel.

$f_t(\omega_i, \omega_t)$ represents the trivial case when no media exists between the illuminant and sensor. Using a delta function, we can assume $f_t = 1$ when $\omega_i = \omega_t$ and $\cos\theta_i = 1$ which leaves the relationship as

$$L_t'(\omega_t) = \frac{L_t(\omega_t) f_t'(\omega_i', \omega_t)\cos\theta_i' d\omega_i'}{d\omega_i}, \tag{5}$$

which gives an accurate way to estimate the transmission of light through a scene without direct measurement.

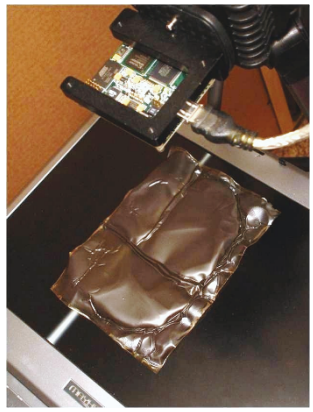

Figure 4: An example scanner configuration.

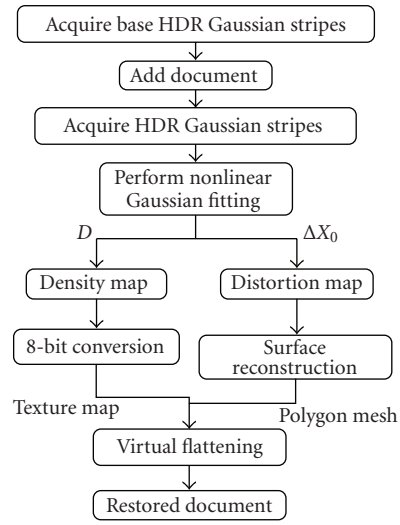

Figure 5: The scanning process.

4. Image-Based Document Scanner

By exploiting the transmissive nature of most document materials, the new image-based acquisition technique presented here provides the direct ability to digitize and restore multilayer photographic negatives. The design of this scanner hinges on the premise that all necessary information in a document can be obtained through rear-illumination of the substrate with visible light.

Additionally, the system requires minimal calibration in the scanning procedure. Many document digitization systems already mentioned in this work require calibration of both the imaging device(s) and illumination source(s). However, this adds to the complexity of operation and may reduce the number of personnel capable of performing a scan. The scanner presented here works in a completely image-based domain, with operations performed on local pixels eliminating the need for global registration or calibration. The scanning is configured by placing a camera above a flat-panel computer monitor as seen in Figure 4.

The data acquired with the image-based scanner allows the optical properties of the negative layers to be decoupled by rear-illuminating the object with time-evolving Gaussian stripes. Two stripes are displayed: a vertical Gaussian stripe given by

$$G(x; x_0, \sigma_x) = ke^{-(x-x_0)^2/2\sigma_x^2} \tag{6}$$

and a horizontal Gaussian stripe given by

$$G\left(y; y_0, \sigma_y\right) = ke^{-(y-y_0)^2/2\sigma_y^2}, \tag{7}$$

where x_0 and y_0 are the means (X_0), σ_x and σ_y are the variance (σ), and k represents the color depth of the display device.

The acquisition system observes two passes of the horizontal and vertical Gaussian stripes. The initial pass is captured with only the display device in the scene to acquire a base case for the Gaussian parameters σ and X_0. The next pass of the stripes is captured with the document in the scene as shown in Figure 4. After the acquisition of four sweeps, calculations are performed on a pixel-by-pixel basis using the time-evolving Gaussian stripes observed for each one (Figure 5). For each pixel, the intensity values are normalized to one, and the scale factor, the Gaussian amplitude α, is saved as the attenuation factor for that pixel. Then a nonlinear Gaussian fit is performed on the normalized intensity values to estimate σ and X_0. This gives two 2D Gaussian functions for each pixel:

$$G\left(x, y : x_0, y_0, \sigma_x, \sigma_y\right) = e^{((x-x_0)^2+(y-y_0)^2)/(\sigma_x+\sigma_y)^2}, \tag{8}$$

$$G\left(x, y : x_0', y_0', \sigma_x', \sigma_y'\right) = e^{((x-x_0')^2+(y-y_0')^2)/(\sigma_x'+\sigma_y')^2}. \tag{9}$$

The optically distorted Gaussian properties σ_x', σ_y', x_0', and y_0' are given by (9). The difference between the Gaussian parameters in (8) and (9) gives an estimation of the optical changes due to the object in the scene.

By inspecting the variations in these parameters one-by-one, it is possible to estimate three unique optical properties from the negative:

(i) amplitude ($\alpha \to \alpha'$): attenuation,

(ii) mean ($X_0 \to X_0'$): surface normal,

(iii) variance ($\sigma \to \sigma'$): density.

However, since the parameters rely on the transmission of the light through large variations in media, the limited dynamic range of the imaging device greatly effects the non-linear fitting.

4.1. Dynamic Range Considerations. When digital cameras image a scene by taking a digital photograph, an analog-to-digital conversion takes place. The main technological element in this process is a charge coupled device (CCD). The CCD measures the irradiance, E, for the duration of exposure time (Δt_e) when an image is captured. However, limited dynamic range of the CCD and quantization in the Analog/Digital conversion often lead to data loss that typically appears as saturation.

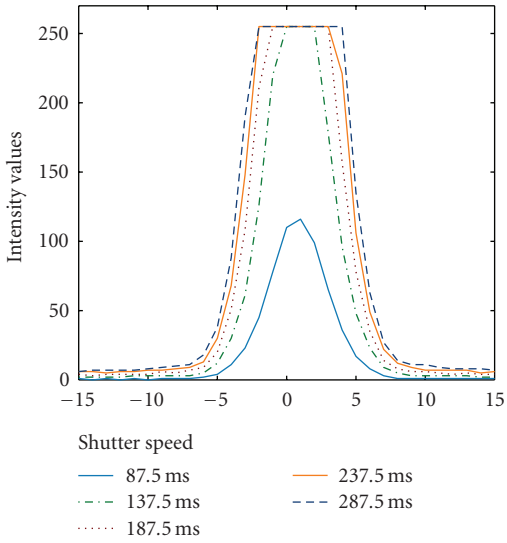

(a) Shows the time-evolving intensity profile of 5 exposures for a single camera pixel using normal 8-bit images

(b) 87.5 ms shutter speed, the left shows illumination without document and the right shows illumination with document in scene

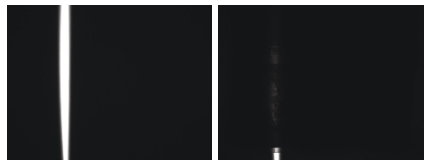

(c) 287.5 ms shutter speed, the left shows illumination without document and the right shows illumination with document in scene

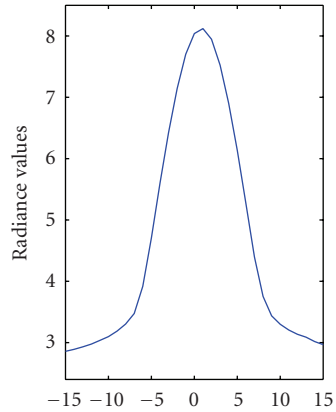

(d) The resultant Gaussian profile in radiance values

Figure 6: The intermediate steps in calculating High Dynamic Range Imaging (HDRI).

A single image captured from the camera, as seen in Figure 6(c), shows the loss of information due to the dynamic range compression. The radiance values at the peak of the Gaussian stripes are all mapped to the same intensity values by the imaging device which greatly reduces the accuracy of Gaussian fitting algorithms. The intensity profile for one pixel at varying exposure rates is shown in Figure 6(a). In this example, all but the fastest shutter speed suffers from data loss. However, to solely use this exposure rate would also be insufficient since there would be data loss for areas with less transmitted light such as when the document is in place which is shown in Figure 6(b).

To compensate for this loss of data, High-Dynamic Range Imaging (HDRI) techniques have been developed. Debevec and Malik [34] extended previous work by acquiring multiple images of the same scene under varying exposure rates. Then the response function for a scene is directly calculated using representative pixels under varying exposures. Once the response function is computed, the set of images can be combined into a floating point radiance map representative of the true radiance in the scene.

The response function is estimated by choosing a single representative pixel that demonstrates a large dynamic range in the scene. Then the image response curve is defined by (10):

$$g\left(I_{(x,e)}\right) = \ln E_x + \ln \Delta t_e. \tag{10}$$

While many digital imaging devices provide response curve customization in hardware, we developed this system to accommodate a wide range of image devices.

4.2. Acquiring Document Content. Correcting photometric distortion in imaged documents that contain folds, creases, and other distortions have previously been addressed [6, 35, 36]. In particular, we have developed two different techniques to reduce these photometric distortions of standard paper documents [3, 4]. However, a more complex model must be used to correct photometric distortion of transparent documents.

The photometric content of the emulsion layer in a photonegative is encoded directly by the relative densities of the silver halide grains. When viewing a planar photonegative under rear-illumination, the resultant image is produced by varying amounts transmitted light due to absorption caused by density variations in the emulsion layer. Reflected light from the base layer can be considered constant which leaves absorption and transmission as the only spatially varying variables when imaging a negative. However, when viewing a negative with a deteriorating base layer, the light transport becomes much more complex.

Reflected light now introduces multiple reductions in the transmitted light due to the non-uniform shape of the base layer and separations, or channels, that form between the emulsion and acetate layers. Typically, the amplitude of transmitted light, α', would be used in a ratio to calculate the attenuation of transmitted light α'/α. However, α' contains error introduced by the acetate layer of the negative. Therefore, another method must be used to extract the density information of only the emulsion layer. We choose a method that factors out the measured intensities and instead uses the change in differential area of radiant exitance to estimate the emulsion density.

The variance of the time-varying Gaussian stripes for each pixel provides a direct method to calculate the differential area on the display device that contributes to the illumination of the document for each pixel in the imaging device. If we consider the variance, σ, for both x and y Gaussian profiles, this effectively creates an elliptical region

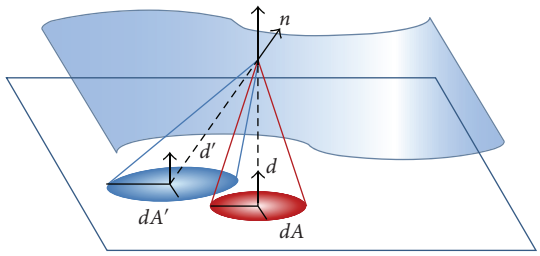

Figure 7: The differential areas of radiance estimated by the variances of both time-varying Gaussians shown on the display surface.

on the display surface as shown in Figure 7. Once both scans are performed, we are left with two ellipses for each imaged pixel: the base contribution ($dA = \pi\sigma_x\sigma_y$) and the negative contribution ($dA' = \pi\sigma_x'\sigma_y'$). The differential solid angle $d\omega$ can be calculated directly from the differential area using $d\omega = dA\cos\theta/d^2$. This can be plugged directly into (5) which gives

$$L_t'(\omega_t) \simeq \frac{L_t(\omega_t) f_t'(\omega_i', \omega_t) dA'}{dA}. \tag{11}$$

Both values of $\cos\theta'$ equal 1 since ω_i', the direction of the solid angle, is parallel to the surface normal as discussed in Section 3.1. Also, as will be discussed in Section 4.3, d and d', the distance between the surface area and the illuminant, are unknown quantities in the image-based implementation, so for estimation $d \simeq d'$.

Next, to estimate the density D, L_t' will be scaled by the measured amplitude of the light transmitted through the negative. By normalizing each pixel transmission by the measured amplitude, we effectively reduce the contribution that the various forms of reflection play in the imaged density. It should also be noted that $f_t'(\omega_i', \omega_t)$ approaches 1 when the transmission is at its maximum. Therefore,

$$D \simeq \frac{L_t(\omega_t) dA'}{dA} \tag{12}$$

is used to reconstruct the photometric content from the emulsion layer. This change in the differential area provides key information in how the transmissivity of the scene has changed when adding the negative and keeping the illumination constant. While we hold to the photographic term density for the reduced transmission induced by the negative, physics and graphics literature typically uses the term absorption synonymously.

We would expect $dA > dA'$ since any additional media in the light path should introduce some form of attenuation. When $dA \gg dA'$, this suggests that there is a much higher opacity due to increased density in the emulsion layer. Consequently, when $dA \simeq dA'$, it can safely be assumed that the pixel contains relatively little information.

Once we acquire the result of (12) for each pixel, we can obtain the *density map* $D_{(u,v)}$. The density map is acquired in floating point values; so a conversion step must take place

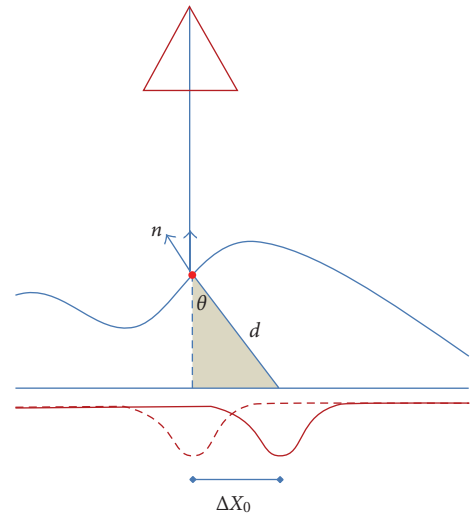

Figure 8: Diffuse Transmission of a back-lit light source where the known-quantity ΔX_0 is used to estimate the surface normal n (dashed line shows observed illumination when negative is not present).

to generate a standard 8-bit greyscale or 32-bit color image using the following:

$$I(u,v) = (D_{(u,v)} + t)s, \tag{13}$$

where t is an intensity translation and s is a scale factor. The values for s and t are determined empirically.

4.3. Distortion Shape Estimation. Continuing the discussion from Section 4.3.2, the diffuse transmission of light can be used to directly estimate the surface orientation for each pixel observation on the document surface. Moreover, for non-planar documents relative variations in surface orientation provide a direct method to estimate local surface shape variations.

The change between the base position of the Gaussian stripe and the modified position provides a basic light-transport model for one or more layered documents. As the time-evolving Gaussian stripe moves across the display device, the observed transmitted intensities will also vary depending on the single-scatter diffusion given in (1). The shifts of the Gaussian peak, given by $(\Delta x_0, \Delta y_0)$, are the pixel-wise orientations used to estimate the orientation of the surface for x and y directions:

$$\theta_x = \arcsin\left(\frac{\Delta x_0}{d_x}\right), \qquad \theta_y = \arcsin\left(\frac{\Delta y_0}{d_y}\right). \tag{14}$$

However, (14) has the unknown quantities d_x and d_y since the surface depth remains unknown as shown in Figure 8. Therefore, for estimation purposes the mean values of both (Δx_0 and Δy_0) are used for d_x and d_y; so (14) becomes

$$\theta_x \simeq \arcsin\left(\frac{\Delta x_0}{\langle \Delta x_0 \rangle}\right), \qquad \theta_y \simeq \arcsin\left(\frac{\Delta y_0}{\langle \Delta y_0 \rangle}\right). \tag{15}$$

To estimate the surface normal, the orientation angles are used in

$$n; \left(\theta_x, \theta_y, 1\right)^T. \tag{16}$$

The normal vector is typically accessed as a unit surface normal where $\sqrt{(n_x^2 + n_y^2 + n_z^2)} = 1$. Then the surface normal can be defined as

$$n \simeq \frac{\left(\theta_x, \theta_y, 1\right)^T}{\sqrt{\left(\theta_x^2 + \theta_y^2 + 1\right)}}. \tag{17}$$

It should be noted that the sign of these normal angles may be globally ambiguous. Similar to the bas-relief ambiguity in shape-from-shading [37], the surface function may be the inverted version of the correct surface.

4.3.1. Surface Reconstruction. Once the surface normals are estimated for each pixel, it is straightforward to calculate the surface gradient at these positions. The surface gradient is defined as $\partial z/\partial x \simeq \theta_x/\sqrt{\theta_x^2 + \theta_y^2 + 1}$ in x and $\partial z/\partial y \simeq \theta_y/\sqrt{\theta_y^2 + \theta_y^2 + 1}$ in y. With known surface gradients, an integrable surface reconstruction, introduced by Frankot and Chellappa [38], can be calculated. Examples of these surfaces are shown in Figures 15(e) and 16(e).

4.3.2. Correcting the Geometric Distortion. By acquiring a 3D map of the emulsion layer, registered to a 2D image of the emulsion density, we are able to apply a *digital flattening* technique we have developed for other applications [2, 7, 39]. This digital flattening is based on a particle system model of the substrate material (originally the substrate was paper on which text is written). The model can be relaxed to assume the shape of a plane, subject to physical modeling constraints on the particles of the model. By enforcing rigidity constraints we can simulate the resulting distortions that come from pushing the non-planar model to a plane. We have shown that this technique can be very accurate at removing depth distortions for page images when the starting 3D model is faithfully acquired.

5. Error

In this work, two major sources of error are encountered. First, the perspective projection of the imaging device adds low-frequency error in X_0. Second, the dynamic range constraints of the imaging device greatly reduced the accuracy of the Gaussian stripe detection.

5.1. Perspective Projection Correction. A global error is introduced into the normal map due to the prospective projection of the imaging system. As the distance from the camera's optical center increases, the angle of incidence on the surface also increases. This creates a systematic shift across the normal map that increases toward the edges of the image. An example of this error when performing a synthetic scan on a plane is shown in Figure 9(d).

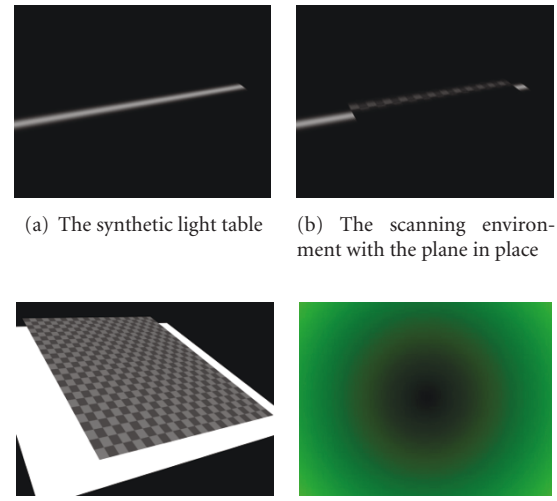

(a) The synthetic light table (b) The scanning environment with the plane in place

(c) The plane on the fully illuminated light table (d) The surface gradients for the plane where lighter intensity shows larger difference in X_0 values

Figure 9: A synthetic scan of a planar object.

To compensate for this error, it is possible to take advantage of the frequency domain where the error occurs. Since the error presents itself as very low-frequency noise, a Gaussian bandpass frequency filter, $H(u, v)$, is applied to the Fourier transform of surface normal components in both the $X(u, v)$ and $Y(u, v)$ directions.

Once the filter is generated, the surface normals may be filtered using $X'(u, v) = X(u, v)H(u, v)$ and $Y'(u, v) = Y(u, v)H(u, v)$. These processed values are then reduced of the error induced by perspective imaging. Therefore, the surface estimation more accurately portrays the actual document shape configuration.

5.2. Error Analysis. To study the accuracy of the scanning system and investigate sources of error, synthetic scans were performed virtually. Utilizing Autodesk 3D Studio Max, environments, closely matching the real-world scanning compositions, were developed to test various aspects of the system.

5.2.1. Synthetic Plane. The first test of the proposed scanning procedure was built using a plane with textured animation that played the sweeping stripe in both directions and a semitransparent plane with a checkerboard texture as seen in Figure 9(c). This test provided the groundwork for estimating the feasibility of the scanner. The planar test demonstrated the noise introduced by the perspective projection of the imaging device. This can be seen by the surface gradients acquired for the plane in Figure 9(d).

To correct the low-frequency noise, the band-pass frequency filters are applied to the surface normal estimations $(\Delta x_0, \Delta y_0)$. Figure 10 shows that the resultant surface as the low-frequency band-pass is increased.

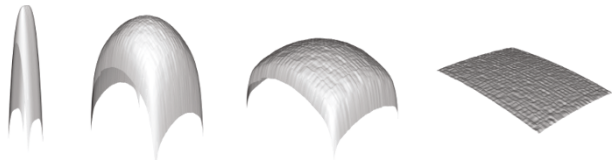

Figure 10: Estimated surface shape with decreasing low-frequency band-pass.

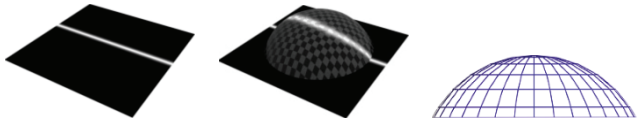

(a) Synthetic illumination device (b) Synthetic scan with sphere in place (c) Side view of the spherical object

Figure 11: A synthetic scan of a hemisphere developed in Autodesk 3D Studio Max.

5.2.2. Synthetic Sphere. Next a semitransparent checkered hemisphere was synthetically scanned. This polygonal hemisphere was placed on the rear-illumination source, Figure 11(a), while a camera observed each of the light stripe positions as seen in Figure 11(b). This scan was performed with 600 stripe positions in both the x and y orientations using a virtual camera with 640×480 resolution. Then, once both $\Delta\sigma$ and ΔX_0 are estimated, the surface is reconstructed using the method described in Section 4.3.1 as shown in Figure 12(b).

To test the accuracy of the scanning and surface reconstruction, the difference between the actual sphere surface and the estimated surface is shown in Figure 12(c). Overall, the results were acceptable for an image-based device.

6. Results

Once the estimation of the synthetic results was satisfactorily obtained, the physical scanner was built using a Windows XP-based 1.6 GHz Pentium M Laptop with a 15″ LCD running at 1024×768 resolution and a 640×480 FireWire greyscale camera obtaining the scan images. By keeping minimal hardware requirements, we hope to make the scanner available to the largest amount of users possible. The scan itself consists of displaying 650 vertical stripes and 400 horizontal stripes for both the base and scanning steps. For each stripe position, 7 images are acquired with decreasing exposure speeds which require 7350 images for each scan. The initial scans took roughly 0.5 second per image capture; so the entire scan took approximately 1 hour. Also, performing the non-linear Gaussian estimation for each pixel required a total of 30 minutes.

The first result of restoring a photographic negative is performed on a recording of a monument. Figure 13(a) shows how the separation between the layers creates channeling with nonuniform transmission of light when the negative is imaged in the normal process. The photometrically corrected negative is shown in Figure 13(d). The surface

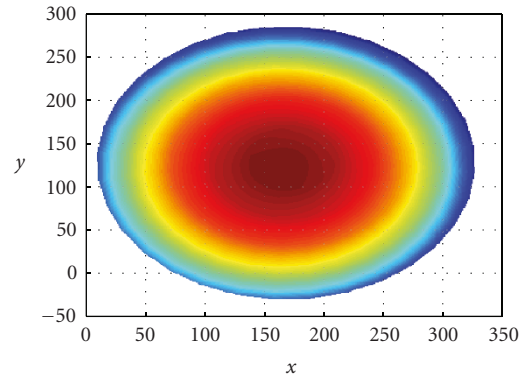

(a) Synthetic sphere depth map

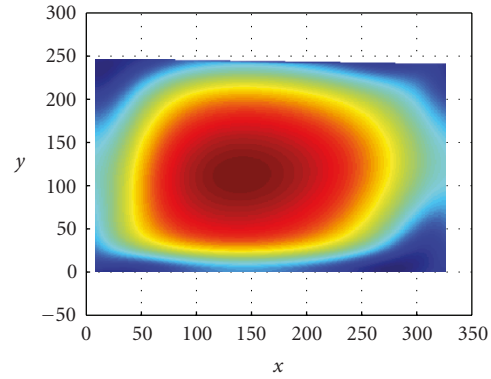

(b) Reconstructed sphere depth map

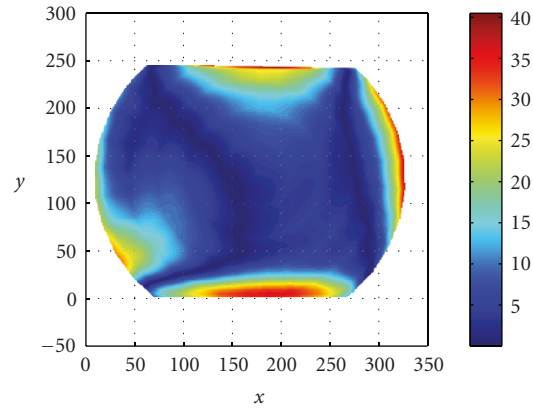

(c) Absolute difference of depth maps

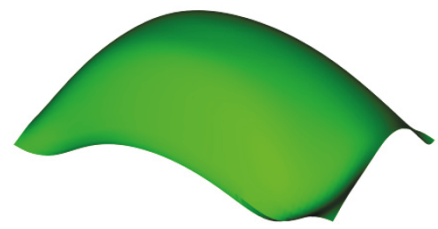

(d) Estimated sphere shape

Figure 12: The analysis of a hemisphere developed in Autodesk 3D Studio Max.

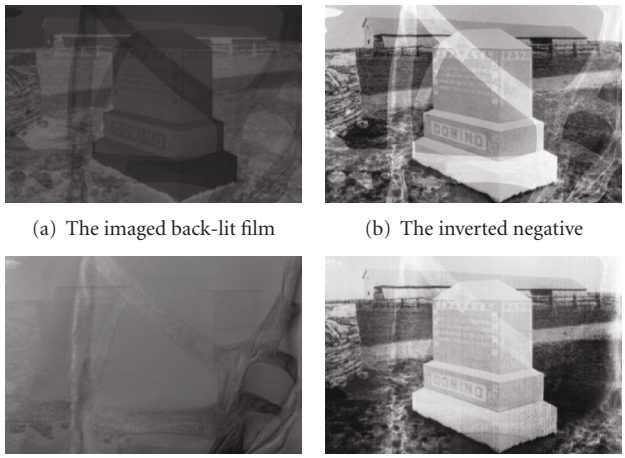

(a) The imaged back-lit film (b) The inverted negative

(c) The estimated surface gradients (d) The photometrically corrected image (density map)

Figure 13: A scan of the negative shown in Figure 2: an example photographic recording of a tombstone.

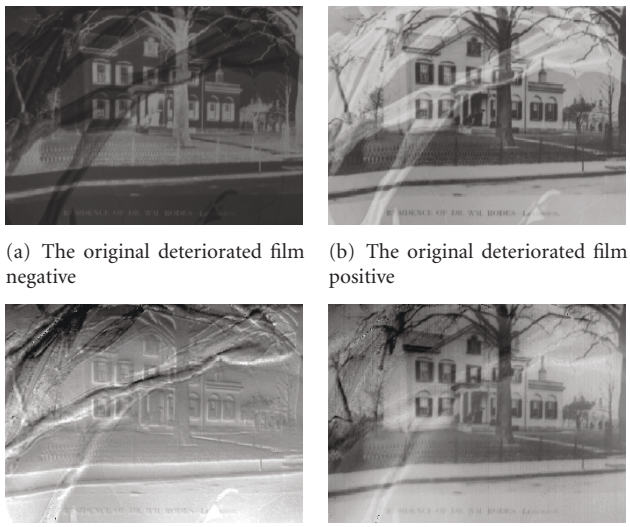

(a) The original deteriorated film negative (b) The original deteriorated film positive

(c) The surface gradient magnitudes (d) The density map

Figure 14: An architectural photographic record from Lexington, Kentucky, USA.

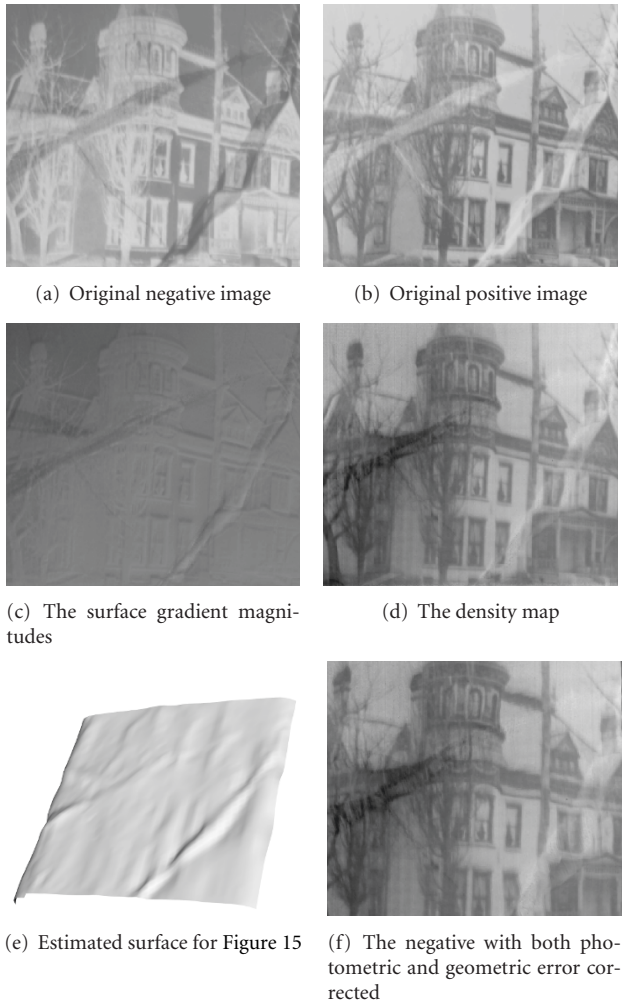

(a) Original negative image (b) Original positive image

(c) The surface gradient magnitudes (d) The density map

(e) Estimated surface for Figure 15 (f) The negative with both photometric and geometric error corrected

Figure 15: Another architectural photographic record from Lexington, Kentucky, USA.

orientations are shown in Figure 13(c). As can be seen by these images, the acquisition process effectively decouples the photographic content from the shape information while excluding attenuation effects caused by the layer separations.

The next example is an architectural recording of a home. Figure 14(b) shows the positive image of the photograph with obvious distortions in photometry and geometry. The photometrically corrected version of the negative is shown in Figure 14(d) and the surface orientations are shown in Figure 14(c).

The third example shows another architectural recording. Again, this negative suffers from the same severe deterioration that is common in acetate film. Figure 15(a) shows the negative acquired with a standard scanning process. The shape information is shown in Figure 15(c) and the content is shown in Figure 15(d). While some areas of the photometric content are restored, there are some areas where the acquisition method failed to accurately capture the negative. We believe that this is mainly due to the low resolution scanning performed on these initial results. Figure 15(e) shows the estimated surface. This geometry is then used for virtual flattening to correct dimensional warping with the result shown in Figure 15(f).

Figure 17(a) shows a closeup of a warped area of the negative from Figure 14. In Figure 17(a), a crack in the emulsion layer is marked in solid white. This area contains some information loss where the material has chipped away, but much of the content remains. It can be seen through the geometric flattening process shown in Figure 17(b) that both sides of the crack are brought back together during restoration. Also, a close-up of Figure 15 shows the resultant geometrically flattened negative in Figure 17(d) with a side-by-side comparison on the unflattened photo (Figure 17(c)).

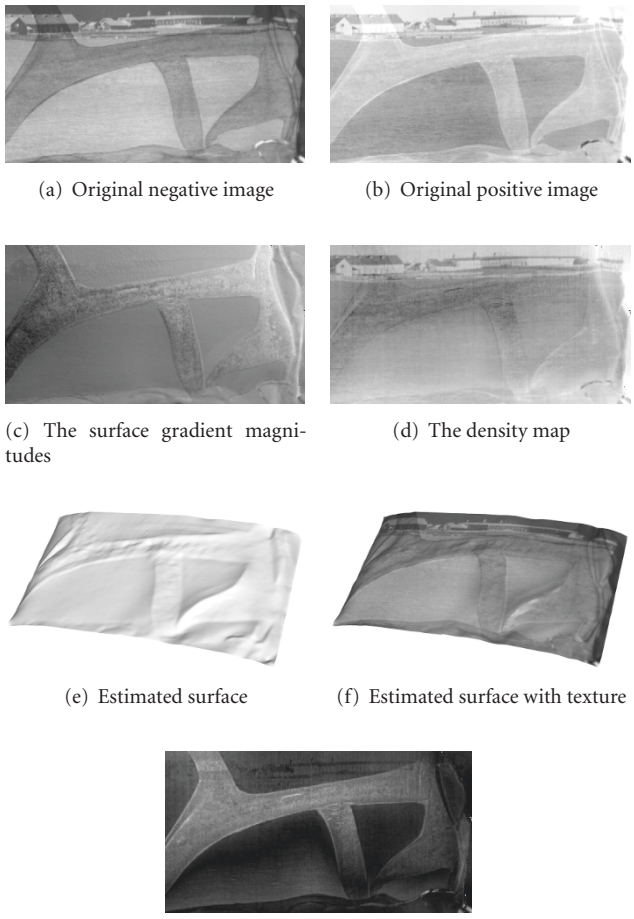

(a) Original negative image

(b) Original positive image

(c) The surface gradient magnitudes

(d) The density map

(e) Estimated surface

(f) Estimated surface with texture

(g) The difference between the original photometric contented and the photometric correction

FIGURE 16: Another architectural photographic record from Lexington, Kentucky, USA.

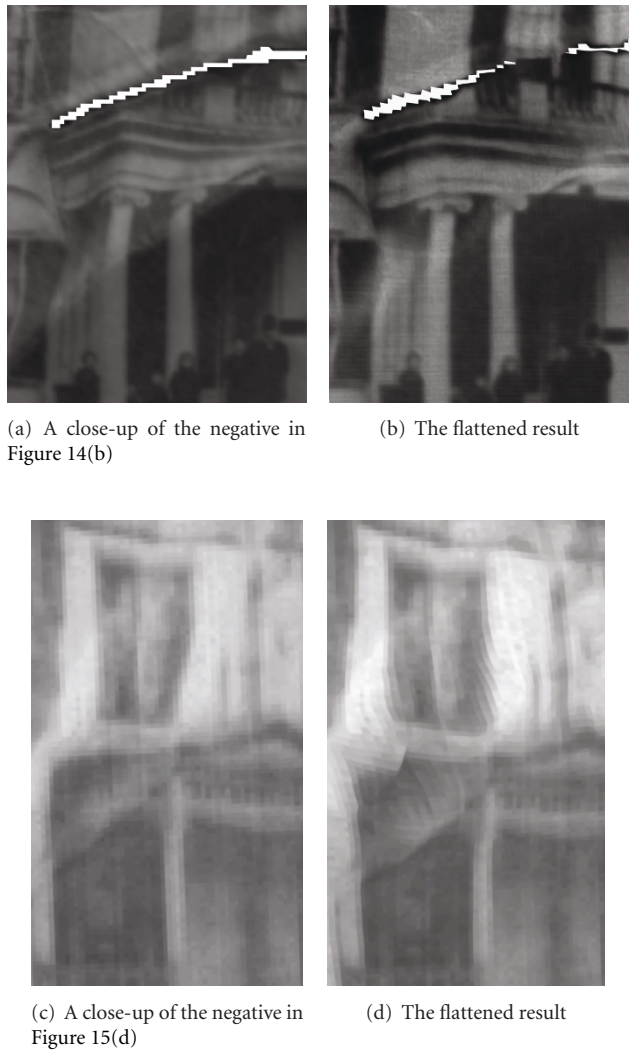

(a) A close-up of the negative in Figure 14(b)

(b) The flattened result

(c) A close-up of the negative in Figure 15(d)

(d) The flattened result

FIGURE 17: The geometric correction of negatives from Figure 14 and Figure 15.

Figure 16 shows the photograph of a farm. Notice the large photometric distortions caused by the large areas of separation between the acetate and emulsion layers in the negative. The is observable in the shape information; see Figures 16(c), 16(e), and 16(f). For clarity, the difference between the the original and photometrically corrected image is shown in Figure 16(g).

7. Future Work

This work will be extended by developing a comprehensive ground-truth analysis suite to provide a metric for the overall restoration accuracy of the system. Moreover, we plan to perform a digital restoration on a deteriorated photonegative and then perform a physical restoration on the negative to provide an accurate ground-truth comparison Also, future work will use more complex structured-light patterns to greatly decrease the acquisition time.

Moreover, increasing both the display and imaging resolution will achieve higher accuracy results. In some initial tests using a higher-resolution camera (2.5 MP) and higher-resolution display (0.8 MP) we were able to generate promising results. Figure 18 shows theses higher-resolution test results. We are convinced by the similarity in texture between Figures 18(b) and 18(e) that these increases in resolution will only improve our results.

Also, we are currently looking into providing ground-truth comparisons by having physical restoration performed on the virtually-restored negatives presented here.

8. Conclusion

In this work, we have demonstrated a cost-effective and fully automatic acquisition system that acquires shape and content information separately for photographic negatives. Using single-scatter diffuse transmission as the basis for the document scanning system, successful results are shown. These complex documents can now be scanned and restored virtually. This presents the first known virtual restoration method for safety negatives.

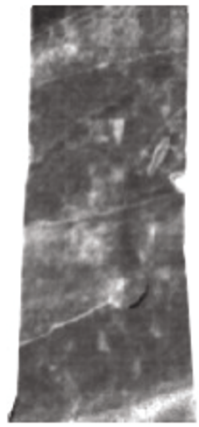

(a) Zoom in of the distorted region

(b) Photometrically correct region

(c) Acquired shape information

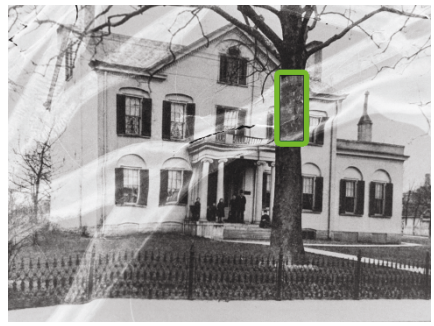

(d) Photographic negative with the region the high-resolution scan marked

(e) An undistorted region from the original negative showing similar content (a tree trunk)

Figure 18: A high-resolution scan of a portion of the negative from Figure 14.

Acknowledgments

The authors would like to thank the University of Kentucky Libraries Special Collections and Digital Programs for access to the acetate safety negatives. They would also like to thank the reviewers for their detailed and constructive comments.

References

[1] L. Zhang, Y. Zhang, and C. Tan, "An improved physically-based method for geometric restoration of distorted document images," *IEEE Transactions on Pattern Analysis and Machine Intelligence*, vol. 30, no. 4, pp. 728–734, 2008.

[2] M. S. Brown and W. B. Seales, "Image restoration of arbitrarily warped documents," *IEEE Transactions on Pattern Analysis and Machine Intelligence*, vol. 26, no. 10, pp. 1295–1306, 2004.

[3] G. V. Landon, Y. Lin, and W. B. Seales, "Towards automatic photometric correction of casually illuminated documents," in *Proceedings of the IEEE Computer Society Conference on Computer Vision and Pattern Recognition (CVPR '07)*, pp. 1–8, Minneapolis, Minn, USA, June 2007.

[4] M. Sun, R. Yang, L. Yun, G. Landon, B. Seales, and M. S. Brown, "Geometric and photometric restoration of distorted documents," in *Proceedings of the 10th IEEE International Conference on Computer Vision (ICCV '05)*, vol. 2, pp. 1117–1123, October 2005.

[5] H. Cao, X. Ding, and C. Liu, "A cylindrical surface model to rectify the bound document image," in *Proceedings of the 9th IEEE International Conference on Computer Vision (ICCV '03)*, vol. 1, pp. 228–233, 2003.

[6] M. S. Brown and Y.-C. Tsoi, "Geometric and shading correction for images of printed materials using boundary," *IEEE Transactions on Image Processing*, vol. 15, no. 6, pp. 1544–1554, 2006.

[7] W. B. Seales and Y. Lin, "Digital restoration using volumetric scanning," in *Proceedings of the 4th ACM/IEEE-CS Joint Conference on Digital Libraries (JCDL '04)*, pp. 117–124, ACM, Tucson, Ariz, USA, June 2004.

[8] D. G. Horvath, *The Acetate Negative Survey: Final Report*, The University of Louisville, Ekstrom Library, Photographic Archives, Louisville, Ky, USA, 1987.

[9] M. Bertalmio, G. Sapiro, V. Caselles, and C. Ballester, "Image inpainting," in *Proceedings of the ACM International Conference on Computer Graphics and Interactive Techniques (SIGGRAPH '00)*, K. Akeley, Ed., pp. 417–424, ACM Press/Addison-Wesley Longman, July 2000.

[10] M. Bertalmio, L. Vese, and G. S. S. Osher, "Simultaneous structure and texture image inpainting," in *Proceedings of the IEEE Computer Society Conference on Computer Vision and Pattern Recognition (CVPR '03)*, vol. 2, pp. 707–712, June 2003.

[11] A. Criminisi, P. Pérez, and K. Toyama, "Region filling and object removal by exemplar-based image inpainting," *IEEE Transactions on Image Processing*, vol. 13, no. 9, pp. 1200–1212, 2004.

[12] S. Roth and M. J. Black, "Fields of experts: a framework for learning image priors," in *Proceedings of the IEEE Computer Society Conference on Computer Vision and Pattern Recognition (CVPR '05)*, vol. 2, pp. 860–867, IEEE Computer Society, San Diego, Calif, USA, June 2005.

[13] E. Ardizzone, H. Dindo, U. Maniscalco, and G. Mazzola, "Damages of digitized historical images as objects for content based applications," in *Proceedings of the 14th European Signal Processing Conference (EUSIPCO '06)*, EURASIP, Florence, Italy, September 2006.

[14] V. Bruni, A. Crawford, A. C. Kokaram, and D. Vitulano, "Digital removal of blotches with variable semitransparency using visibility laws," in *Proceedings of the 2nd International Symposium on Advances in Brain, Vision, and Artificial Intelligence (BVAI '07)*, pp. 254–263, Naples, Italy, October 2007.

[15] R. Szeliski, S. Avidan, and P. Anandan, "Layer extraction from multiple images containing reflections and transparency," in *Proceedings of the IEEE Computer Society Conference on Computer Vision and Pattern Recognition (CVPR '00)*, vol. 1, pp. 246–253, 2000.

[16] F. Stanco, G. Ramponi, and A. de Polo, "Towards the automated restoration of old photographic prints: a survey," in *Proceedings of the IEEE Region 8 Computer as a Tool (EUROCON '03)*, vol. 2, pp. 370–374, September 2003.

[17] R. Pintus, T. Malzbender, O. Wang, R. Bergman, H. Nachlieli, and G. Ruckenstein, "Photo repair and 3D structure from flatbed scanners," in *Proceedings of the 4th International Conference on Computer Vision Theory and Applications (VISAPP '09)*, vol. 1, pp. 40–50, Lisboa, Portugal, February 2009.

[18] F. Stanco, L. Tenze, G. Ramponi, and A. de Polo, "Virtual restoration of fragmented glass plate photographs," in *Proceedings of the 12th IEEE Mediterranean Electrotechnical Conference (MELECON '04)*, vol. 1, pp. 243–246, Dubrovnik, Yugoslavia, May 2004.

[19] M. Ben-Ezra and S. K. Nayar, "What does motion reveal about transparency?" in *Proceedings of the 9th IEEE International Conference on Computer Vision (ICCV '03)*, vol. 2, pp. 1025–1032, Nice, France, October 2003.

[20] N. J. W. Morris and K. N. Kutulakos, "Reconstructing the surface of inhomogeneous transparent scenes by scatter-trace photography," in *Proceedings of the 11th IEEE International Conference on Computer Vision (ICCV '07)*, pp. 1–8, October 2007.

[21] G. Eren, O. Aubreton, F. Meriaudeau, et al., "Scanning from heating: 3D shape estimation of transparent objects from local surface heating," *Optics Express*, vol. 17, no. 14, pp. 11457–11468, 2009.

[22] D. E. Zongker, D. M. Werner, B. Curless, and D. H. Salesin, "Environment matting and compositing," in *Proceedings of the 26th Annual Conference on Computer Graphics and Interactive Techniques*, pp. 205–214, ACM Press/Addison-Wesley, New York, NY, USA, 1999.

[23] Y.-Y. Chuang, D. E. Zongker, J. Hindorff, B. Curless, D. H. Salesin, and R. Szeliski, "Environment matting extensions: towards higher accuracy and realtime capture," in *Proceedings of the 27th Annual Conference on Computer Graphics and Interactive Techniques*, pp. 121–130, ACM Press/Addison-Wesley, New York, NY, USA, 2000.

[24] G. V. Landon, W. B. Seales, and D. Clarke, "A new system to acquire and restore document shape and content," in *Proceedings of the 5th ACM/IEEE International Workshop on Projector Camera Systems (PROCAMS '08)*, pp. 1–8, ACM, Marina del Rey, Calif, USA, August 2008.

[25] Chicago Albumen Works, http://www.albumenworks.com/Detacetatefilms.html.

[26] L. Wang, W. Wang, J. Dorsey, X. Yang, B. Guo, and H.-Y. Shum, "Real-time rendering of plant leaves," in *Proceedings of the International Conference on Computer Graphics and Interactive Techniques (SIGGRAPH '06)*, p. 5, ACM, Boston, Mass, USA, July-August 2006.

[27] A. Gardner, C. Tchou, T. Hawkins, and P. Debevec, "Linear light source reflectometry," *ACM Transactions on Graphics*, vol. 22, no. 3, pp. 749–758, 2003.

[28] M. Mudge, J.-P. Voutaz, C. Schroer, and M. Lum, "Reflection transformation imaging and virtual representations of coins from the hospice of the grand st. bernard," in *Proceedings of the 6th International Symposium on Virtual Reality, Archaeology and Cultural Heritage (VAST '05)*, pp. 29–39, 2005.

[29] S. Chandrasekhar, *Radiative Transfer*, Dover, New York, NY, USA, 1960.

[30] J. R. Frisvad, N. J. Christensen, and P. Falster, "Efficient light scattering through thin semi-transparent objects," in *Proceedings of the 3rd International Conference on Computer Graphics and Interactive Techniques in Australasia and Southeast Asia (GRAPHITE '05)*, pp. 135–138, ACM, Dunedin, New Zealand, November-December 2005.

[31] Y. M. Govaerts, S. Jacquemoud, M. M. Verstraete, and S. L. Ustin, "Three-dimensional radiation transfermodeling in a dicotyledon leaf," *Applied Optics*, vol. 35, pp. 6585–6598, 1996.

[32] B. D. Ganapol, L. F. Johnson, P. D. Hammer, C. A. Hlavka, and D. L. Peterson, "LEAFMOD: a new within-leaf radiative transfer model," *Remote Sensing of Environment*, vol. 63, no. 2, pp. 182–193, 1998.

[33] J. Gu, R. Ramamoorthi, P. Belhumeur, and S. Nayar, "Dirty glass: rendering contamination on transparent surfaces," in *Proceedings of the 18th Eurographics Workshop on Rendering Techniques*, pp. 159–170, June 2007.

[34] P. E. Debevec and J. Malik, "Recovering high dynamic range radiancemaps from photographs," in *Proceedings of the 24th Annual Conference on Computer Graphics and Interactive Techniques*, pp. 369–378, August 1997.

[35] T. Wada, H. Ukida, and T. Matsuyama, "Shape from shading with interreflections under a proximal light source: distortion-free copying of an unfolded book," *International Journal of Computer Vision*, vol. 24, no. 2, pp. 125–135, 1997.

[36] E. Prados, F. Camilli, and O. Faugeras, "A unifying and rigorous shape from shading method adapted to realistic data and applications," *Journal of Mathematical Imaging and Vision*, vol. 25, no. 3, pp. 307–328, 2006.

[37] P. N. Belhumeur, D. J. Kriegman, and A. L. Yuille, "The bas-relief ambiguity," *International Journal of Computer Vision*, vol. 35, no. 1, pp. 33–44, 1999.

[38] R. T. Frankot and R. Chellappa, "A method for enforcing integrability in shape fromshading algorithms," *IEEE Transactions on Pattern Analysis and Machine Intelligence*, vol. 10, no. 4, pp. 439–451, 1988.

[39] M. S. Brown and W. B. Seales, "Document restoration using 3D shape: a general deskewing algorithm for arbitrarily warped documents," in *Proceedings of the IEEE International Conference on Computer Vision (ICCV '01)*, vol. 2, pp. 367–374, 2001.